

DualContrast: Unsupervised Disentangling of Content and Transformations with Implicit Parameterization

Mostofa Rafid Uddin¹, Min Xu¹✉

¹ Ray and Stephanie Lane Computational Biology Department,
Carnegie Mellon University, Pittsburgh, PA 15213, USA
✉ Corresponding Author: mxu1@cs.cmu.edu

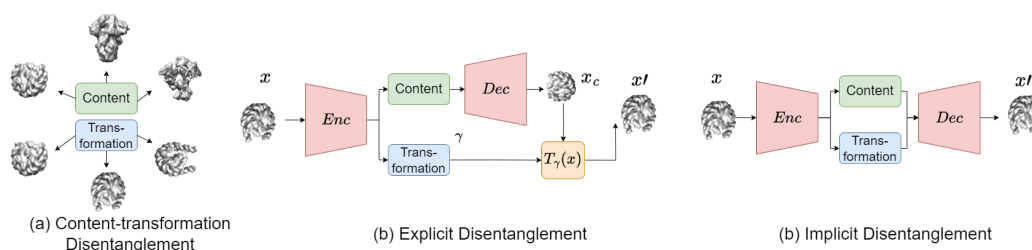


Figure 1: Conceptualization of content-transformation disentanglement (a) and comparison between **existing** explicit (b) and **our** implicit (c) unsupervised methods. Both of these methods optimize content and transformation latent spaces while reconstructing x' from x . However, explicit methods use the transformation space to infer a fixed parameter set γ and use it to transform the feature map/image x_c generated by conditioning the decoder on content space. On the contrary, our implicit method conditions the decoder on both content and transformation to generate image x' and does not restrict the transformation space to a fixed set of parameters.

Abstract

Unsupervised disentanglement of content and transformation has recently drawn much research, given their efficacy in solving downstream unsupervised tasks like clustering, alignment, and shape analysis. This problem is particularly important for analyzing shape-focused real-world scientific image datasets, given their significant relevance to downstream tasks. The existing works address the problem by explicitly parameterizing the transformation factors, significantly reducing their expressiveness. Moreover, they are not applicable in cases where transformations can not be readily parameterized. An alternative to such explicit approaches is self-supervised methods with data augmentation, which implicitly disentangles transformations and content. We demonstrate that the existing self-supervised methods with data augmentation result in the poor disentanglement of content and transformations in real-world scenarios. Therefore, we developed a novel self-supervised method, DualContrast, specifically for unsupervised disentanglement of content and transformations in shape-focused image datasets. Our extensive experiments showcase the superiority of DualContrast over existing self-supervised and explicit parameterization approaches. We leveraged DualContrast to disentangle protein identities and protein conformations in cellular 3D protein images. Moreover, we also disentangled transformations in MNIST, viewpoint in the Linemod Object dataset, and human movement deformation in the Starman dataset as transformations using DualContrast.

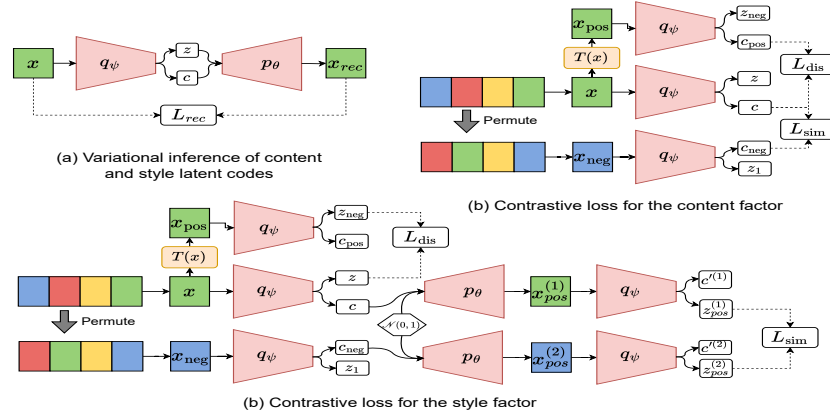


Figure 2: Our proposed contrastive learning-based unsupervised content-transformation disentanglement pipeline. (a) The variational inference of content and transformation factors with L_{VAE} . (b,c) The contrastive strategy to create positive and negative pairs w.r.t. content (b) and transformation factors (c), respectively. DualContrast combines the three parts and is trained end-to-end.

1 Introduction

In many real-world image datasets, particularly in scientific imaging domains, the object shapes being visualized may undergo multiple transformations [1, 2]. These shape-focused image datasets can thus be regarded as samples generated from two independent factors, one representing the semantic attribute termed content and the other representing the transformations. Content is regarded as the *form* of an object being visualized in the image [1] that is unaltered after applying any nuisance transformation. On the other hand, transformation dictates the specific *state* or *realization* of that form of the object. Taking proteins inside the cells as an example, changing the transformation factor changes the conformation of the protein where the protein identity (*i.e.*, protein composition) does not change (Figure 1). On the other hand, changing the content factor is analogous to changing the proteins from one identity to another through compositional change. Such a phenomenon holds for many real-world shape-focused datasets. Disentangling content and transformation factors of images can significantly facilitate several downstream tasks, including clustering [3], alignment [4, 2], zero-shot transfer [5], bias removal [6, 7], cross-domain retrieval [8, 9], shape analysis [10, 11, 4, 2, 3], etc. [11].

A number of works have been done to directly or indirectly solve the content-transformation disentanglement problem [12, 8, 10, 1, 4, 2], whereas many of them use annotated factors for training. However, such annotation is hard to obtain, and thus, unsupervised disentanglement methods are desired. Only a few works [1, 2, 4] have addressed the problem in a completely unsupervised setting. Among them, VITAE [1] performed explicit parameterization of transformation factors as diffeomorphic transformations and achieved noteworthy disentanglement of content and transformation in several image datasets. SpatialVAE [2] and Harmony [4] focus on representing known transformation types as transformation factors. SpatialVAE [2] performed disentanglement of two-dimensional translation and rotation, whereas Harmony [4] demonstrated disentanglement of a broader set of transformations that can be explicitly parameterized.

Though these unsupervised explicit parameterization methods have demonstrated several successes, they have several major limitations in general: (1) These method uses the transformation factor to generate only a few parameterized transformations. In reality, many transformations do not have a well-defined parameterized form, e.g., protein conformation changes, viewpoint change (LineMod), human deformation during movement (Starmen), etc. These explicit methods can not disentangle such transformation by design. (2) They use Spatial Transformer Networks (STN) [13] for inferring the transformation factor, which requires a continuous parameterization of the transformation to be disentangled. The continuity of many transformations (*e.g.*, $SO(3)$ rotation) in neural networks is often a concern [14]. Moreover, (3) these methods often infer spurious contents during disentanglement in real-world datasets (Fig. 3). Due to these limitations, an unsupervised content-transformation disentanglement method without explicit transformation representation is much desired.

Consequently, in this work, we focused on the more generalized setting of unsupervised content-transformation disentanglement without any explicit parameterization of the transformation factor. Given the theoretical study by Von et al. [15] showing the implicit disentanglement ability of standard Contrastive Learning (CL) methods, e.g., SimCLR [16], to disentangle content from style, a plausible solution could be using SimCLR with geometric data augmentation for our implicit content-transformation disentanglement task. However, these popular CL methods [16] have rarely achieved disentanglement in practice [6], and we also found that SimCLR with geometric data augmentation performs poorly in our shape-focused image datasets of interest (Table 1).

To this end, we develop a novel contrastive learning method for implicit content-transformation disentanglement, termed “DualContrast”. Similar to previous content-transformation disentangling methods [17, 2, 1, 4], it is a deep generative model based on a variational autoencoder (VAE) architecture. However, unlike previous methods, it does not require labels or explicit parameterization of any latent factor. Instead, it uses a novel contrastive strategy that creates “positive” and “negative” contrastive pairs w.r.t. both content and transformation latent factor. We create negative pairs w.r.t. transformation factor and positive pairs w.r.t. content factor by simply rotating the samples. In addition, we randomly permute the samples in the batch to create a negative pair for a batch of samples w.r.t. content latent factor. Without prior knowledge, creating positive pairs w.r.t. the transformation latent factor from the input samples is not possible. To this end, we generate samples from an identical distribution of the transformation representations in the embedding space and treat them as positive pairs for the transformation latent factor. Upon creating both “positive” and “negative” pairs w.r.t. both factors, we penalize similarity between negative pairs and distance between positive pairs for each factor. In *DualContrast*, we combine these contrastive losses with VAE reconstruction loss and train the model in an end-to-end manner.

With such a strategy, by just performing simple rotation to create contrastive pairs, DualContrast disentangles a much wider range of more complicated transformations, e.g., human deformation in starmen, viewpoint in Linemod, the writing style in MNIST, etc. With DualContrast, we, for the first time, solved the scientific problem of disentangling protein identities from protein conformations in simulated 3D protein images (Figure 7) inside the cell, known as cellular cryo-ET subtomograms. DualContrast could successfully disentangle the protein identities as content and protein conformations as transformation factors in simulated subtomograms, which is not achievable with previous methods. Overall, our qualitative and quantitative experimental results show the efficacy of DualContrast in isolating content from transformation compared to existing relevant methods.

A summary of our contributions is as follows:

- We work on a challenging setting of learning unsupervised disentangled representations of content and transformation in shape-focused images by removing the requirement of explicit parameterization.
- We develop a novel contrastive generative modeling strategy that creates positive-negative pairs for both content and transformation latent factors. We introduced a novel way of designing contrastive pairs for transformation factors.
- We show that DualContrast is highly effective in disentangling a wide range of transformations from the content in various shape-focused image datasets by only using simple rotation for creating contrastive pairs.
- Leveraging DualContrast, we, for the first time, disentangled protein identities (*i.e.* composition) from protein conformations in simulated 3D cellular cryo-ET subtomograms, as a proof of principle.

2 Related Works

Disentangled Representation Learning: Our method can be regarded as a disentangled representation learning method that disentangles generative factors of variation as content-specific and transformation-specific factors. There exist many generic disentangled representation learning approaches [18, 17, 19, 20, 21, 22] where the factors of variations are interpreted by traversing through the learned factors and reconstructing samples. However, these methods do not perform very well in specifically disentangling content and transformation factors [1]. To this end, specialized methods that deal with such two factors have been introduced recently. Many of them [23, 12, 8] are partially or weakly supervised and use labels associated with one of the latent factors to train their models.

However, these methods are not applicable when such supervision is unavailable beforehand, which is often the case for many real-life datasets. There are a few [1, 4, 2, 15] approaches that deal with the unsupervised disentanglement of content and transformation. However, these methods perform explicit parameterization of the transformation factor as affine or some specific parameterized transformation. In contrast, our method does not impose any explicit parameterization on the transformation latent factor and does not face the issues of the explicit methods (Section 1).

Contrastive Learning based Disentanglement: Contrastive learning is the primary building block of our method. Contrastive Learning with data augmentation with existing approaches, *e.g.*, InfoNCE loss-based SimCLR [16], etc., has been previously used by [15, 8] to isolate content from style. Though in several scenarios, style in shape focused images can be referred to as transformations, these works do not specifically focus on shape-focused real-world images. Moreover, our experiments demonstrate that SimCLR with rotation augmentation in a standard encoder-decoder framework leads to very poor disentanglement of content and transformation (Table 1). Moreover, [15] only creates positive pairs w.r.t content and negative pair w.r.t. style with data augmentation in SimCLR. We have observed this scheme does not work well in our scenario. Unlike these works, our approach uses a novel strategy to create “negative” and “positive” pairs for both content and transformation of latent factors without any InfoNCE loss.

Unsupervised Content-style disentanglement: Apart from [15], several methods [6, 24, 25, 26, 27, 28] exist that perform unsupervised content-style disentanglement, focusing on natural images. These methods focus on the controllable generation of realistic natural images, mostly using ImageNet pretrained models. Unlike these methods, our work primarily focuses on disentangling content and transformation in shape-focused image datasets. Moreover, we do not depend on any ImageNet pretrained models as our images of interest differ greatly from the natural images of ImageNet.

Protein Composition-Conformation Disentanglement: One of the major contributions of our work is disentangling protein identity characterized by large compositional variability as the content factor and protein states characterized by conformational variability or subtle compositional variability as transformation factor from 3D cellular cryo-electron tomography (cryo-ET) subimages or subtomograms. Previously, Harmony [4] was used to disentangle large compositional variability in cellular subtomograms. HEMNMA-3D [29] and TomoFlow [30] were used to disentangle subtle compositional or conformational variability in subtomograms using known templates. SpatialVAE [2] disentangled subtle conformational variability from 2D cryo-EM images. There exists several works on single particle cryo-EM and cryo-ET reconstruction, *e.g.*, cryoDRGN2 [31], cryoFIRE [3], cryoAI [32], etc. that performs amortized inference of transformation ($SO(3) \times d^2$) and latent space representing content. However, these works mainly focus on 2D-to-3D reconstruction instead of content-transformation disentanglement. Ours is the first work to deal with both large and subtle compositional variability in two different latent spaces for 3D cryo-ET subtomograms.

3 Method

3.1 Disentangling Content and Transformation

Disentangling content and transformation refers to learning one mapping $h : \mathcal{X} \rightarrow \mathcal{C} \times \mathcal{Z}$, where \mathcal{X} is an input space, \mathcal{C} and \mathcal{Z} are the intermediary content and transformation representation spaces respectively. Here, h can be decomposed as $h_c : \mathcal{X} \rightarrow \mathcal{C}$ and $h_z : \mathcal{X} \rightarrow \mathcal{Z}$ representing the content and transformation mapping, respectively. In an unsupervised setting, distinguishing between content and transformation can be tricky. In this paper, we distinguish between content and transformation with respect to a family of transformations $\mathcal{T} : \mathcal{X} \rightarrow \mathcal{X}$ such that the following two conditions hold:

- **Condition 1:** $\forall T \in \mathcal{T}$, s.t., for any $\mathbf{x} \in \mathcal{X}$, $h_c(T(\mathbf{x})) = h_c(\mathbf{x})$.
- **Condition 2:** $\exists T \in \mathcal{T}$, s.t., for any $\mathbf{x}^{(1)}, \mathbf{x}^{(2)} \in \mathcal{X}$, $h_z(T(\mathbf{x}^{(1)})) = h_z(\mathbf{x}^{(2)})$.

Condition 1 defines content space which is invariant w.r.t. \mathcal{T} . On the other hand, **condition 2** states that there is a $T \in \mathcal{T}$ that can make the transformation of any two samples equal when applied to any one of them. Thus it defines transformation space which is informative of \mathcal{T} .

For content-transformation disentangling, changes in \mathcal{C} must be unaffected by changes in \mathcal{Z} and vice versa. In our problem setting, no labels associated with content space \mathcal{C} or transformation space \mathcal{Z}

are known. The exact family of transformation \mathcal{T} is also not known beforehand. Thus, we aim to simultaneously learn the family of transformations \mathcal{T} and the content factors unaltered by \mathcal{T} .

3.2 Method Overview and Notation

Our method is built upon a variational auto-encoder (VAE) based architecture (Figure 2), where we perform inference of the content and transformation factors in the data. Consider, a sample space \mathcal{X} , two latent distribution spaces Φ_Z and Φ_C , two latent spaces \mathcal{Z} and \mathcal{C} . We apply an encoder network $q_\psi : \mathcal{X} \rightarrow \mathcal{C} \times \mathcal{Z}$ on a sample space $bx \in \mathcal{X}$ to encode content distribution $\phi_c \in \Phi_c$ and transformation distribution $\phi_z \in \Phi_z$, where $(\phi_c, \phi_z) = q_\psi(\mathbf{x})$. Latent parameters $\mathbf{c} \in \mathcal{C}$, $\mathbf{z} \in \mathcal{Z}$ are drawn from distributions ϕ_c and ϕ_z respectively. These parameters are then decoded using a decoder network $p_\theta : \mathcal{C} \times \mathcal{Z} \rightarrow \mathcal{X}$ to produce $x_{\text{recon}} = p_\theta(\mathbf{c}, \mathbf{z})$.

3.3 Variational Inference of Content and Transformation Factors

Similar to a variational auto-encoder (VAE) setting, the encoder and decoder network parameters are simultaneously optimized to maximize the variational lower bound to the likelihood $p(\mathbf{x})$ called the evidence lower bound (ELBO). ELBO maximizes the log-likelihood of the data and minimizes the KL divergence between latent distributions and a prior distribution. The objective function for this can be written as:

$$\begin{aligned} p(\mathbf{x}) &\geq \mathbb{E}_{q_\psi(\mathbf{c}, \mathbf{z}|\mathbf{x})} \left[\log \frac{p_\theta(\mathbf{x}, \mathbf{c}, \mathbf{z})}{q_\psi(\mathbf{c}, \mathbf{z}|\mathbf{x})} \right] \\ &= \mathbb{E}_{q_\psi(\mathbf{c}, \mathbf{z}|\mathbf{x})} \log p_\theta(\mathbf{x}|\mathbf{c}, \mathbf{z}) - KL(q_\psi(\mathbf{c}|\mathbf{x})||p(\mathbf{c})) - KL(q_\psi(\mathbf{z}|\mathbf{x})||p(\mathbf{z})). \end{aligned} \quad (1)$$

The log-likelihood term is maximized using a reconstruction loss L_{recon} . The prior for \mathbf{c} and \mathbf{z} , $p(\mathbf{c})$ and $p(\mathbf{z})$ respectively are assumed to be standard normal distribution. In short, we write the KL terms as $L_{\text{KL}(\mathbf{c})}$ and $L_{\text{KL}(\mathbf{z})}$. To regularize the effect of prior on the final objective separately for two latent factors, we scale the two losses with two hyperparameters γ_c and γ_z . Our loss function for variational inference becomes:

$$L_{\text{vae}} = L_{\text{rec}} + \gamma_c L_{\text{KL}(\mathbf{c})} + \gamma_z L_{\text{KL}(\mathbf{z})}. \quad (2)$$

We observe that by deactivating the KL term associated with any one of the factors, the likelihood tends to be optimized through the other latent factor. For instance, if γ_c is set as 0 and γ_z has a large value, then the L_{rec} is optimized through \mathbf{c} only. As a consequence, \mathbf{c} captures all the information in \mathbf{x} , whereas \mathbf{z} becomes totally independent of the data. In such a scenario, \mathbf{z} will be a random factor with no relation to the transformation factor of the data, which is not desirable.

3.4 Creating Contrastive Pair with respect to Content Latent Factor

We adopt a contrastive strategy for content-transformation disentanglement. We first develop a strategy to impose a structure to the content latent factor with contrastive learning. To this end, we create negative and positive pairs for each data sample w.r.t. the content factor. Hence, we randomly pick two samples \mathbf{x} and $\mathbf{x}_{\text{neg}(\mathbf{c})}$, where $\mathbf{x}, \mathbf{x}_{\text{neg}(\mathbf{c})} \in \mathcal{X}$ and regard them as negative pairs of each other w.r.t the content factor. Such strategy is commonly used in traditional self-supervised learning approaches [16, 33]. Considering the high heterogeneity present in the dataset, evidenced by a large number of classes, this approach accounts for the likelihood that any two randomly selected samples will have different content. To generate positive pairs w.r.t. the content factor, we pick any sample \mathbf{x} and transform it with a transformation $T \in \mathcal{T}$ to generate $\mathbf{x}_{\text{pos}(\mathbf{c})}$. We use the encoder q_ψ to generate content factors \mathbf{c} , \mathbf{c}_{pos} , and \mathbf{c}_{neg} respectively from \mathbf{x} , $\mathbf{x}_{\text{pos}(\mathbf{c})}$, and $\mathbf{x}_{\text{neg}(\mathbf{c})}$. We use a contrastive loss to penalize the distance between \mathbf{c} and \mathbf{c}_{pos} and the similarity between \mathbf{c} and \mathbf{c}_{neg} . Our contrastive loss for content latent factor can be written as:

$$L_{\text{con}(\mathbf{c})} = L_{\text{dist}}(\mathbf{c}, \mathbf{c}_{\text{pos}}) + L_{\text{sim}}(\mathbf{c}, \mathbf{c}_{\text{neg}}) \quad (3)$$

To implement L_{dist} and L_{sim} , we use mean absolute cosine distance and mean absolute cosine similarity, respectively.

3.5 Creating Contrastive Pair with respect to Transformation Latent Factor

Imposing contrastive loss on the content latent factor satisfies condition 1 of the content-transformation disentanglement (Section 3.1). However, the content-transformation disentanglement remains only partial since it does not satisfy condition 2. To solve this issue, we design another contrastive loss w.r.t. the transformation latent factor. Designing a contrastive loss that explicitly enforces condition 2 is not possible, given the transformation that may equalize the transformation factor of two samples can not be approximated. To this end, we design a contrastive loss that implicitly encourages condition 2. We validated the design experimentally in Section 4.

The negative pair of a sample $\mathbf{x} \in \mathcal{X}$ w.r.t. transformation latent factor is generated while creating a positive pair of it w.r.t content factor. This is because a transformation T on \mathbf{x} alters its transformation, but not its contents. So, we regard $\mathbf{x}_{\text{pos}(\mathbf{c})}$ as $\mathbf{x}_{\text{neg}(\mathbf{z})}$. However, creating positive pairs of samples w.r.t. transformation is very challenging as they can not be created in the input space, unlike others. To this end, we adopted a strategy of creating pairs of samples from the same distribution in the transformation factor embedding space. We randomly sample $\mathbf{z}^{(1)}$ and $\mathbf{z}^{(2)}$ from $\mathcal{N}(0, 1)$ and use the decoder p_θ to generate samples $\mathbf{x}_{\text{pos}(\mathbf{z})}^{(1)}$ and $\mathbf{x}_{\text{pos}(\mathbf{z})}^{(2)}$ from them (Fig. 2 (c)). In the decoder, as content input, we use content factor $\mathbf{c}^{(1)}$ and $\mathbf{c}^{(2)}$ obtained by encoding two random samples $\mathbf{x}^{(1)}$ and $\mathbf{x}^{(2)}$. Consequently, $\mathbf{x}_{\text{pos}(\mathbf{z})}^{(1)} = p_\theta(\mathbf{c}^{(1)}, \mathbf{z}^{(1)})$ and $\mathbf{x}_{\text{pos}(\mathbf{z})}^{(2)} = p_\theta(\mathbf{c}^{(2)}, \mathbf{z}^{(2)})$ serve as the positive pairs w.r.t. transformation latent factor. We then use the encoder q_ψ to generate \mathbf{z} , \mathbf{z}_{neg} , $\mathbf{z}_{\text{pos}}^{(1)}$, and $\mathbf{z}_{\text{pos}}^{(2)}$ from \mathbf{x} , $\mathbf{x}_{\text{neg}(\mathbf{z})}$, $\mathbf{x}_{\text{pos}(\mathbf{z})}^{(1)}$, and $\mathbf{x}_{\text{pos}(\mathbf{z})}^{(2)}$ respectively. We use a contrastive loss to penalize the distance between $\mathbf{z}_{\text{pos}}^{(1)}$ and $\mathbf{z}_{\text{pos}}^{(2)}$ and similarity between \mathbf{z} and \mathbf{z}_{neg} . Our contrastive loss for transformation latent factor can be written as:

$$L_{\text{con}(\mathbf{z})} = L_{\text{dist}}(\mathbf{z}_{\text{pos}}^{(1)}, \mathbf{z}_{\text{pos}}^{(2)}) + L_{\text{sim}}(\mathbf{z}, \mathbf{z}_{\text{neg}}) \tag{4}$$

Similar to $L_{\text{con}(\mathbf{c})}$, we use mean absolute cosine distance and mean absolute cosine similarity to implement L_{dist} and L_{sim} , respectively.

Objective Function: In summary, we train the encoder and decoder networks by simultaneously minimizing the loss components. Our overall objective function to minimize is:

$$L = L_{\text{vae}} + L_{\text{con}(\mathbf{c})} + L_{\text{con}(\mathbf{z})} \tag{5}$$

4 Experiments & Results

Benchmark Datasets: We report results on MNIST [34], LineMod [35], Starmen [36], and a realistically simulated protein subtomogram dataset. Only LineMod features RGB images among these datasets, while the other three consist of grayscale images. The subtomogram is a 3D volumetric dataset, whereas the others are 2D images.

Baselines: We used the unsupervised content-transformation disentanglement methods, SpatialVAE [2], Harmony [4], VITAE [1] with explicit parameterization and InfoNCE loss based standard self-supervised learning method with rotation augmentation [15] as baseline approaches. Several generic disentangled representation learning methods, such as beta-VAE, Factor-VAE, beta-TCVAE, DIP-VAE, etc., are available that do not aim to disentangle specific factors such as content or transformation in the data but rather aim to disentangle all factors of variation. However, previous studies [2, 1] have shown that such methods perform worse than methods specifically aiming to disentangle content and transformation. Therefore, we did not use these methods as baselines in our experiments.

Implementation Details: We implemented the encoder using a Convolutional Neural Network (CNN) and the decoder using a Fully Connected Network (FCN). Our experiments used the same latent dimension for content and transformation factors, except for Harmony [4] and SpatialVAE [2], where a specific dimension needs to be used for transformation latent factors. We train our models for 200 epochs with a learning rate of 0.0001 in NVIDIA RTX A500 GPUs and AMD Raedon GPUs. We optimize the model parameters with Adam optimizer.

Table 1: Quantitative Results of unsupervised Content-Transformation Disentangling Methods on MNIST and LineMod datasets. This evaluation only shows the disentanglement performance w.r.t ground truth content factors. We report mean \pm std. dev. over model training by setting 3 different random seeds. Here, for Harmony and SpatialVAE, the transformation latent factor is restricted to dimension 3. For the other methods, there is no such restriction on the transformation latent factor. For SimCLR, (Disc) means discriminative model (without any reconstruction), and (Gen) means Generative model (with reconstruction).

| Method | MNIST | | LineMod | |
|---|-----------------------------------|-------------------------------------|-----------------------------------|-------------------------------------|
| | $D_{\text{score}}(c c)(\uparrow)$ | $D_{\text{score}}(c s)(\downarrow)$ | $D_{\text{score}}(c c)(\uparrow)$ | $D_{\text{score}}(c s)(\downarrow)$ |
| SpatialVAE [2] | 0.81 ± 0.01 | 0.28 ± 0.02 | 0.95 ± 0.02 | 0.32 ± 0.01 |
| Harmony [4] | 0.82 ± 0.01 | 0.31 ± 0.02 | 0.90 ± 0.01 | 0.56 ± 0.02 |
| SimCLR (Disc) with rotation [15] | 0.58 ± 0.01 | 0.60 ± 0.01 | 0.62 ± 0.01 | 0.40 ± 0.01 |
| SimCLR (Gen) with rotation [15] | 0.53 ± 0.01 | 0.67 ± 0.02 | 0.61 ± 0.02 | 0.79 ± 0.01 |
| VAE with two latent space | 0.63 ± 0.00 | 0.63 ± 0.00 | 0.87 ± 0.00 | 0.87 ± 0.00 |
| VITAE [1] | 0.77 ± 0.00 | 0.32 ± 0.00 | 0.92 ± 0.00 | 0.90 ± 0.00 |
| DualContrast (w/o $L_{\text{con}(c)}$) | 0.87 ± 0.02 | 0.21 ± 0.02 | 0.86 ± 0.01 | 0.31 ± 0.02 |
| DualContrast (w/o $L_{\text{con}(z)}$) | 0.79 ± 0.04 | 0.85 ± 0.02 | 0.79 ± 0.03 | 0.86 ± 0.03 |
| DualContrast | 0.89 ± 0.01 | 0.31 ± 0.02 | 0.95 ± 0.01 | 0.48 ± 0.02 |

Evaluation Metrics: We assess DualContrast based on two criteria: (1) the quantitative disentanglement of content and transformation factors and (2) the qualitative capability of image generation through content-transformation transfer.

For (1), there exists several metrics, *e.g.*, MIG score, D_{score} , etc. Locatello et al [37] demonstrated that these metrics are highly correlated. To this end, similar to [1], we only use D_{score} to measure the disentanglement. D_{score} is simply a measurement of how well the ground truth factors can be predicted from the corresponding latent factors. In our scenario, there are four such quantities - (a) predictivity of content labels given content factor $D_{\text{score}}(c|c)$ or transformation factor $D_{\text{score}}(c|s)$ (b) predictivity of transformation labels given content factor $D_{\text{score}}(s|c)$ or transformation factor $D_{\text{score}}(s|s)$. For MNIST and LineMod, we do not have any transformation labels, so we only reported values for (a). Similar to [15], we use linear Logistic Regression Classifiers to measure predictivity (D_{score}) across all our experiments.

The quantitative measurement, particularly when transformation labels are not available, might be misleading. To this end, we perform qualitative evaluation by generating images while transferring content and transformation from original images from the dataset. We take a set of K images \mathbf{x} and create a $K \times K$ grid of K^2 images using the different combinations of content and transformation factors from those K images. In the grid, we keep the content factor and transformation factor consistent across the columns and the rows respectively. In other words, the image at position (i, j) in the grid is generated using the content of image x_j and transformation of image x_i . For the protein subtomogram dataset, we also provide qualitative results through embedding visualization (Figure 9).

4.1 DualContrast disentangles writing style from MNIST handwritten digit images

Similar to [4, 2, 1], we start our experiments with the MNIST dataset of handwritten digits. We performed a quantitative comparison between DualContrast and the baseline approaches, as shown in Table 1. We observed that DualContrast achieves higher $D_{\text{score}}(c|c)$ compared to other explicitly parameterized approaches [4, 2, 1].

However, since transformation labels are not present for MNIST, relying entirely on the content prediction performance for disentanglement might be misleading. For example, the degenerate solution achieves even lower $D_{\text{score}}(c|s)$ as transformation does not represent anything. To this end, we report qualitative results for baseline methods and our approach DualContrast (Fig. 3). In generating images with varying content and styles, we observe that Harmony, SpatialVAE, and C-VITAE generate many images with erroneous content and styles. On the other hand, DualContrast produces a few minor errors and no extreme mistakes. We also include tSNE embedding of the content factors inferred by the models on the MNIST test dataset associated with class labels (Figure 4). On the embedding space, DualContrast clearly shows superior clustering performance. All of

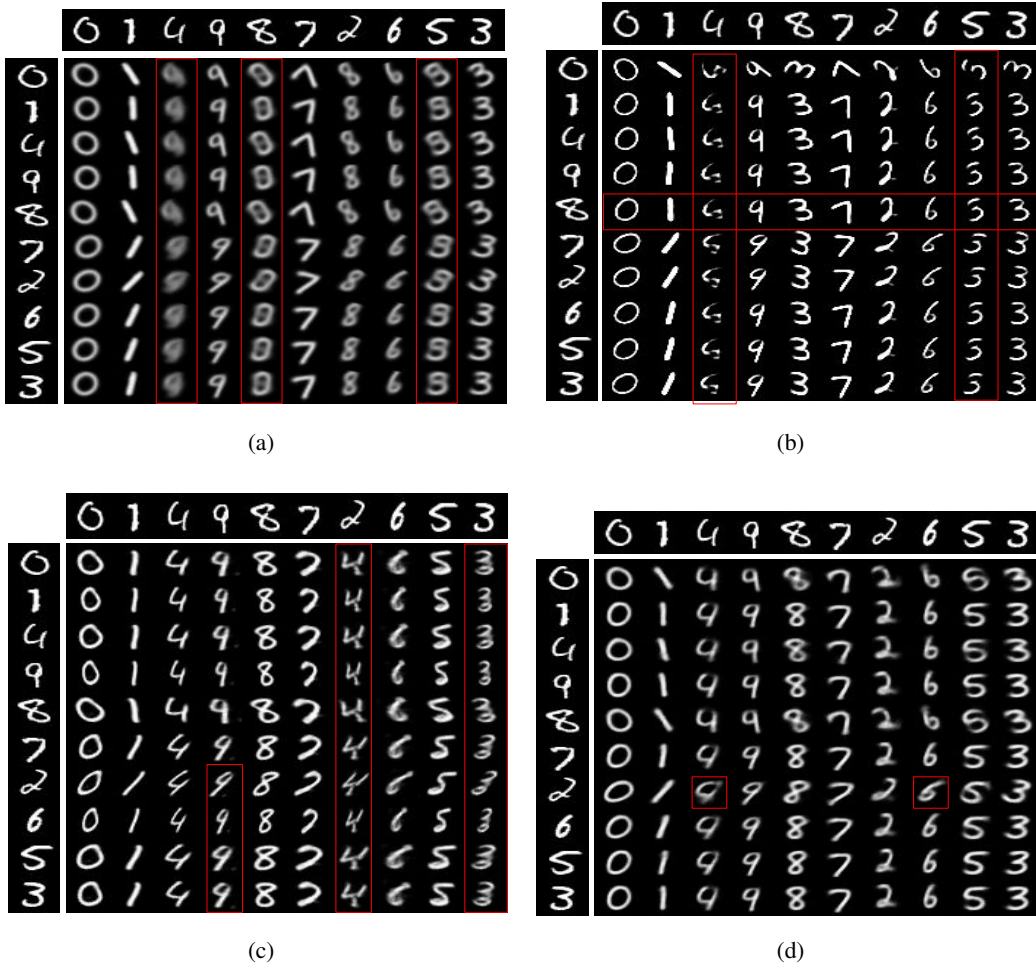


Figure 3: Qualitative content-transformation transfer based image generation results for MNIST. (a), (b), (c), and (d) shows the results with Harmony [4], Spatial-VAE [2], VITAE [1], and DualContrast respectively. Erroneous generations (both in terms of content and transformation) are marked within red boxes.

these suggest better content-transformation disentanglement with our approach than existing explicit parameterization approaches.

4.2 DualContrast Disentangles ViewPoint from Linemod Object Dataset

LineMod is an RGB object recognition and 3D pose estimation dataset [35] with 15 unique object types. It contains 15 unique objects: ‘ape’, ‘bench vise’, ‘bowl’, ‘cam’, ‘can’, ‘cat’, ‘cup’, ‘driller’, ‘duck’, ‘eggbox’, ‘glue’, ‘hole puncher’, ‘iron’, ‘lamp’ and ‘phone’, photographed in a highly cluttered environment. We use a synthetic version of the dataset [38], which has the same objects rendered under different viewpoints. The dataset is publicly available at this url. The dataset has 1,313 images per object category. We used 1,000 images per category for training and the remaining for testing.

We evaluated the disentanglement scores D_{score} (Table 1) for DualContrast and baseline approaches, where DualContrast clearly shows the best performance. We used the object identities as content labels during the evaluation.

We also performed qualitative measurement with image transfer and depicted the result of DualContrast and its most relevant (in terms of the generality of transformations) VITAE in Fig 5. We observe that VITAE distorts the images significantly while performing image generation with content-style

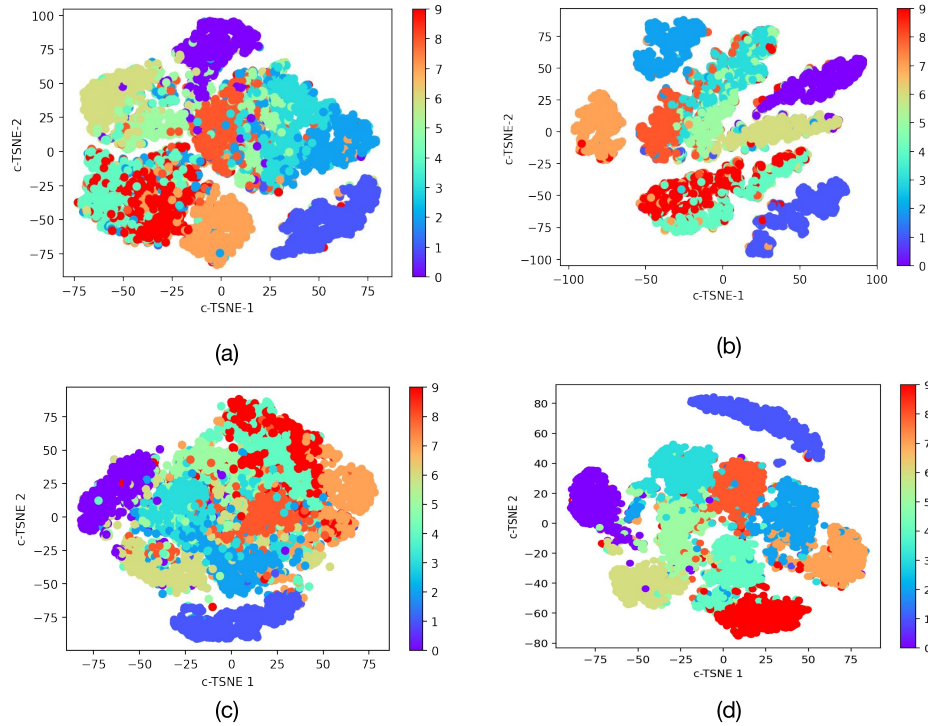


Figure 4: tSNE embedding plots of content latent factor learned by the unsupervised content-style disentanglement methods. (a), (b), (c), and (d) shows the results for Harmony [4], Spatial-VAE [2], C-VITAE [1], and DualContrast respectively. Overall, DualContrast shows superior performance.

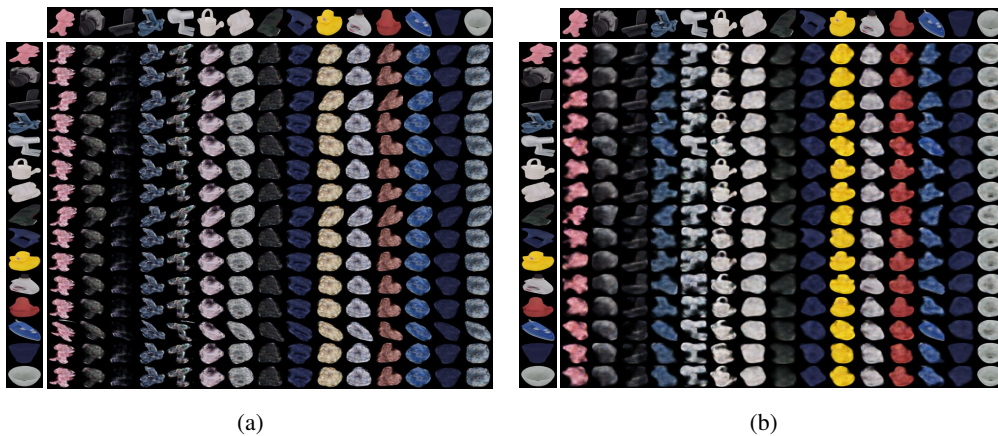


Figure 5: Qualitative Results of Unsupervised Content-Transformation Disentanglement on LineMod obtained by VITAE[1] (a) and DualContrast (b), respectively.

transfer. On the other hand, DualContrast does not face such issues. Moreover, DualContrast can disentangle different viewpoints of the objects as the transformation factor using only 2D rotation to create contrastive pairs in its model.

4.3 DualContrast disentangles Human Deformation from starmen shapes dataset

Starmen is a 2D synthetic shape dataset of the deformable human body [36] consisting of 10,000 shape-focused images, which is publicly available at <https://zenodo.org/records/5081988>

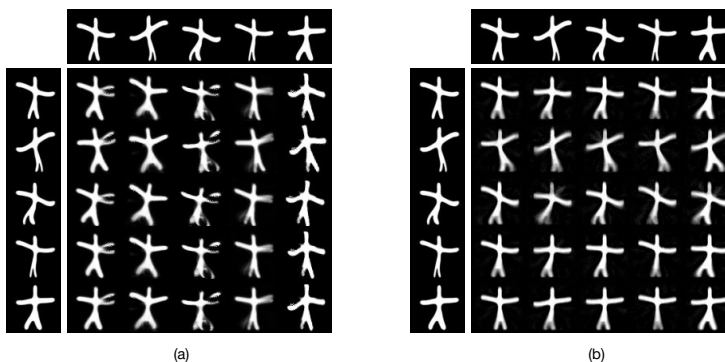


Figure 6: Qualitative Results of Unsupervised Content-Transformation Disentanglement on Starmen (a) and (b) shows the results obtained with VITAE [1] and DualContrast, respectively.

under CC-BY license. Each starmen image is a grayscale image of size 64×64 . They are generated by deforming five control points (two on arms, two on legs, one on head) on template human shapes.

We randomly took 6,000 starmen images to train our models and kept the remaining 4,000 for testing. We report the qualitative results by VITAE [1] and DualContrast in Figure 6. From the image generation results with the content-transformation transfer, we can observe that DualContrast disentangles the deformation of starmen shapes as transformation and the identity (based on leg thickness) as content, providing a smooth image generation result. On the other hand, VITAE [1] does not perform such meaningful content-transformation disentanglement, generating implausible results.

4.4 DualContrast Disentangles Protein Identity from states in Cryo-ET Subtomograms

We created a realistic simulated cryo-ET subtomogram dataset of 18,000 subtomograms of size 32^3 . The dataset consists of 3 protein classes of similar sizes- Nucleosomes, Sars-Cov-2 spike protein, and Fatty Acid Synthase Unit. These proteins are significantly different in terms of their composition, which determines their different identities. Moreover, structures for all of these three types of proteins have been resolved in cellular cryo-ET [39, 30, 40], which makes it feasible to use them for our study. Moreover, cellular cryo-ET is the primary method to capture these proteins inside the cells in their native state [41].

For each protein class, we collected 6 different protein structures from the RCSB PDB website [42]. RCSB PDB is a web server containing the structure of millions of proteins. For nucleosomes, we collected PDB IDs ‘2pyo’, ‘7kbe’, ‘7pex’, ‘7pey’, ‘7xzy’, and ‘7y00’. All of these are different conformations of nucleosomes that slightly vary in composition (Figure ??). For sars-cov-2 spike proteins, we collected PDB IDs ‘6vxx’, ‘6vyb’, ‘6xr8’, ‘6xra’, ‘6zox’, and ‘6zp0’. Among them, only ‘6xra’ shows much variation in structure from the other ones, and the rest of the PDB IDs are very similar in structure. For Fatty Acid Synthase (FAS) Unit, we used PDB IDs ‘8prv’, ‘8ps1’, ‘8ps9’, ‘8psj’, ‘8psm’, ‘8psp’. They also vary very slightly in terms of the structure.

After collecting these 18 PDB structures as PDB files, we used EMAN PDB2MRC [43] to create density maps (as MRC file extension) from the PDB files. We create density maps of size 32^3 with 1 nm resolution. We then randomly rotate and translate each density map and create 1000 such copies. We then convolve the density maps with CTF with CTF parameters common in experimental datasets (Defocus -5 nm, Spherical Aberration 1.7, Voltage 300 kV). Afterward, we add noise to the convolved density maps so that the SNR is close to 0.1. Thus, we prepare 18,000 realistic subtomograms with 3 different protein identities, each with 6 different conformations. We uploaded the entire dataset anonymously at <https://zenodo.org/records/11244440> under CC-BY-SA license. 3D slice-by-slice visualizations for sample subtomograms for nucleosomes, spike proteins, and FAS units are provided in Figure 7.

We trained DualContrast and baseline approaches against the protein subtomogram dataset. We could not train VITAE [1] on subtomogram datasets since it did not define any transformation for 3D data. Designing CPAB transformation for 3D data by ourselves was challenging. Among the other baseline

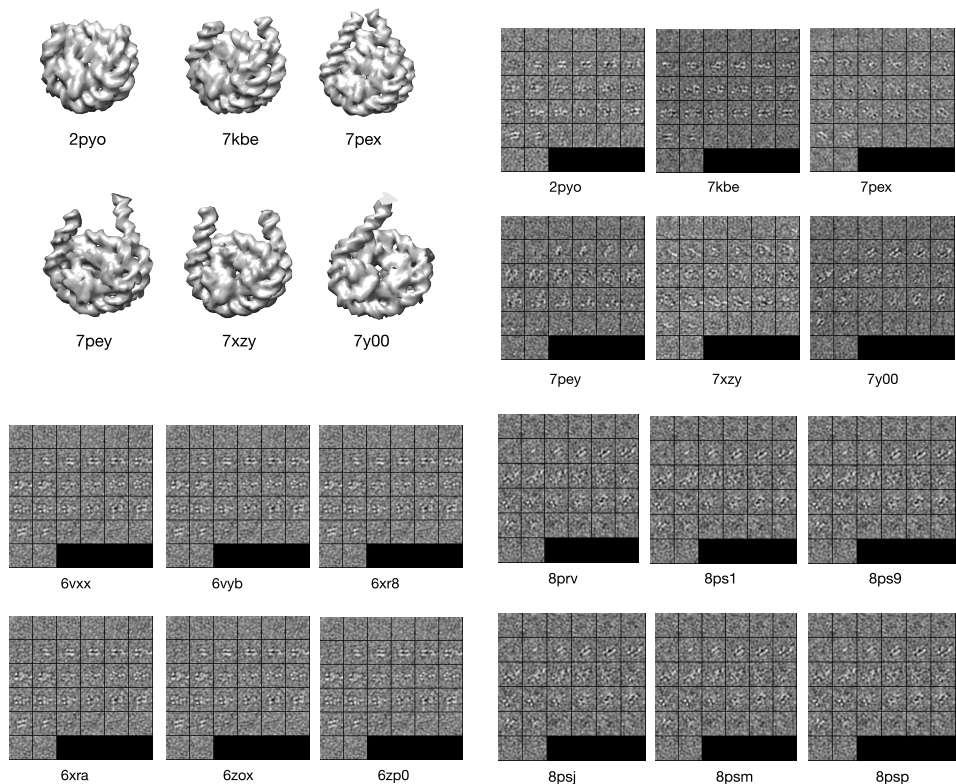


Figure 7: (a) Isosurface visualization of Nucleosome Density Maps. Each density map slightly varies in terms of conformation. They are associated with the PDB IDs in the figure. (b) 3D Slice by slice visualization of several subtomograms of the corresponding nucleosome density maps.

approaches, spatialVAE could not distinguish the protein identities with high heterogeneity at all, which is evident by its embedding space UMAP (Figure 8). Only Harmony provided somewhat plausible results apart from DualContrast.

We observed that the DualContrast content factor perfectly clustered the three protein identities from the dataset (GMM clustering accuracy 0.99), profoundly disentangling the transformations (Figure 9(b)). We do not see such perfect clustering for Harmony (Figure 9(a)); rather, protein identities with very different compositions get mixed up due to their conformational variation (GMM clustering accuracy 0.70). We further observe that DualContrast transformation embedding clusters have similar nucleosome conformations, showing disentanglement of conformation from protein identity. On the other hand, in Harmony, the transformation factor only represents rotation and translation by design and can not capture nucleosome conformations. Moreover, even its content embedding for manually selected (not through automatic clustering) nucleosome subtomograms can not show good clustering of conformations (Figure 9(b)).

Ablation Study: To evaluate the individual contribution of the contrastive losses, we conduct both quantitative and qualitative ablation analyses of DualContrast. We trained (1) DualContrast without

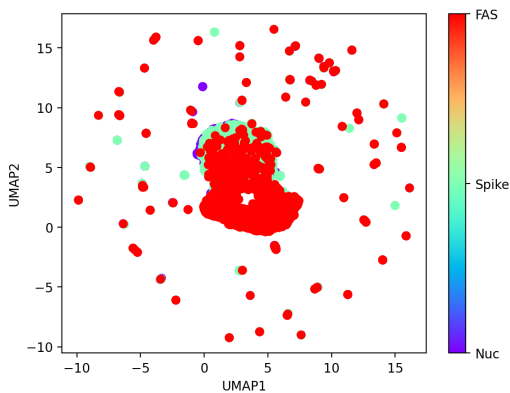


Figure 8: UMAP of content factor learned by SpatialVAE [2] on our subtomogram dataset. The protein identities are indistinguishable from the embedding space.

any contrastive loss, which is basically a VAE with two latent spaces, (2) DualContrast with only $L = L_{\text{VAE}} + L_{\text{con}(z)}$, and (3) $L = L_{\text{VAE}} + L_{\text{con}(c)}$. We qualitatively and quantitatively evaluated each model. We show the quantitative results in Table 1 and qualitative results of MNIST in Figure 10.

For (1), the D_{score} is almost the same for both content and transformation factors, indicating equal predictivity of the digit classes by both factors. This is obvious given that the model has no inductive bias to make different factors capture different information. In model (2), using contrastive loss w.r.t. only transformation factor z makes it uninformative of the data. Thus, it provides a small $D(c|z)$ score as desired, but the changing z does not affect the image generation (Figure 10). On the other hand, in the model (3), using contrastive loss w.r.t. only content factor c gives a less informative content factor, a lower $D(c|c)$ score, and a higher $D(c|z)$ score, contrary to what is desired. These results indicate contrastive loss w.r.t to both factors is crucial to get the desired disentanglement.

5 Limitation

Similar to existing content-transformation disentanglement methods [2, 4, 1, 8, 12], DualContrast is applicable to data samples with single objects. This is reasonable, given content and transformation can not be defined for data with multiple objects. Moreover, we limited our study only to shape-focused image datasets, motivated by the problem of conformation disentanglement of protein subtomograms. Consequently, we only used rotation to create contrastive pairs, which worked pretty well in our cases. For image datasets where appearance or illumination plays a crucial role, using only rotation to create contrastive pairs may not work well. However, disentanglement in natural image datasets is a different scenario that is outside of the scope of this paper.

6 Conclusion

This work focuses on a challenging setting of the unsupervised content-transformation disentanglement problem in shape-focused image datasets, where the transformation latent factor is not explicitly parameterized. To tackle this problem, we propose a novel method termed DualContrast. DualContrast employs generative modeling with a novel contrastive learning strategy that creates positive

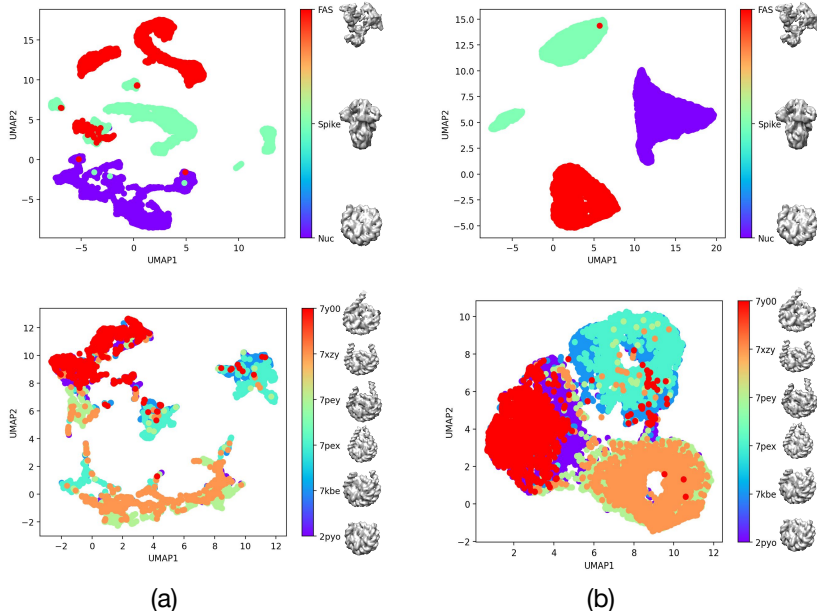


Figure 9: Disentanglement of composition and conformations in cellular subtomogram dataset. (a) UMAP embedding of the content factor of all subtomograms (top) and only nucleosome subtomograms (bottom) with Harmony [4] (b) UMAP embedding of the content factor (top) and transformation factor (bottom) obtained by DualContrast.

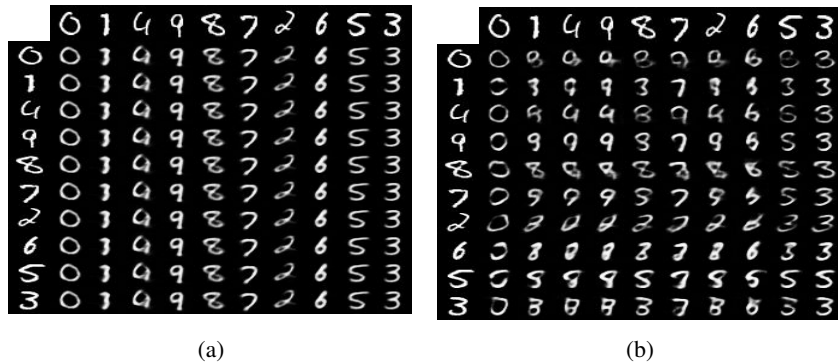


Figure 10: Content-transformation transfer results from ablation analysis. (a) and (b) shows the results when the model is trained with $L_{\text{VAE}} + L_{\text{con}(z)}$ and $L_{\text{VAE}} + L_{\text{con}(c)}$ respectively.

and negative pairs for content and transformation latent factors. Our extensive experiments show DualContrast’s effective disentanglement of challenging transformation factors across various shape-based image datasets; including simulated cellular subtomograms, where it solved the unexplored problem of isolation of protein conformations from protein identities, as proof of principle.

7 Acknowledgement

This work was supported in part by U.S. NIH grants R01GM134020 and P41GM103712, NSF grants DBI-1949629, DBI-2238093, IIS-2007595, IIS-2211597, and MCB-2205148. This work was supported in part by Oracle Cloud credits and related resources provided by Oracle for Research, and the computational resources support from AMD HPC Fund. MRU were supported in part by a fellowship from CMU CMLH.

References

- [1] Nicki Skafté and Søren Hauberg. Explicit disentanglement of appearance and perspective in generative models. *Advances in Neural Information Processing Systems*, 32, 2019.
- [2] Tristan Bepler, Ellen Zhong, Kotaro Kelley, Edward Brignole, and Bonnie Berger. Explicitly disentangling image content from translation and rotation with spatial-vae. *Advances in Neural Information Processing Systems*, 32, 2019.
- [3] Axel Levy, Gordon Wetzstein, Julien NP Martel, Frederic Poitevin, and Ellen Zhong. Amortized inference for heterogeneous reconstruction in cryo-em. *Advances in neural information processing systems*, 35:13038–13049, 2022.
- [4] Mostofa Rafid Uddin, Gregory Howe, Xiangrui Zeng, and Min Xu. Harmony: A generic unsupervised approach for disentangling semantic content from parameterized transformations. In *Proceedings of the IEEE/CVF Conference on Computer Vision and Pattern Recognition*, pages 20646–20655, 2022.
- [5] Keyang Zhou, Bharat Lal Bhatnagar, and Gerard Pons-Moll. Unsupervised shape and pose disentanglement for 3d meshes. In *Computer Vision—ECCV 2020: 16th European Conference, Glasgow, UK, August 23–28, 2020, Proceedings, Part XXII 16*, pages 341–357. Springer, 2020.
- [6] Lilian Ngweta, Subha Maity, Alex Gittens, Yuekai Sun, and Mikhail Yurochkin. Simple disentanglement of style and content in visual representations. In *International Conference on Machine Learning*, pages 26063–26086. PMLR, 2023.
- [7] Jungsoo Lee, Eungyeup Kim, Juyoung Lee, Jihyeon Lee, and Jaegul Choo. Learning debiased representation via disentangled feature augmentation. *Advances in Neural Information Processing Systems*, 34:25123–25133, 2021.
- [8] Jonathan Kahana and Yedid Hoshen. A contrastive objective for learning disentangled representations. In *European Conference on Computer Vision*, pages 579–595. Springer, 2022.
- [9] Zoe Piran, Niv Cohen, Yedid Hoshen, and Mor Nitzan. Disentanglement of single-cell data with biolord. *Nature Biotechnology*, pages 1–6, 2024.
- [10] Luca Cosmo, Antonio Norelli, Oshri Halimi, Ron Kimmel, and Emanuele Rodola. Limp: Learning latent shape representations with metric preservation priors. In *Computer Vision—ECCV 2020: 16th European Conference, Glasgow, UK, August 23–28, 2020, Proceedings, Part III 16*, pages 19–35. Springer, 2020.
- [11] Xiao Liu, Pedro Sanchez, Spyridon Thermos, Alison Q O’Neil, and Sotirios A Tsaftaris. Learning disentangled representations in the imaging domain. *Medical Image Analysis*, 80:102516, 2022.
- [12] Ananya Harsh Jha, Saket Anand, Maneesh Singh, and VS Rao Veeravasarapu. Disentangling factors of variation with cycle-consistent variational auto-encoders. In *Proceedings of the European Conference on Computer Vision (ECCV)*, pages 805–820, 2018.
- [13] Max Jaderberg, Karen Simonyan, Andrew Zisserman, et al. Spatial transformer networks. *Advances in neural information processing systems*, 28, 2015.
- [14] Yi Zhou, Connelly Barnes, Jingwan Lu, Jimei Yang, and Hao Li. On the continuity of rotation representations in neural networks. In *Proceedings of the IEEE/CVF conference on computer vision and pattern recognition*, pages 5745–5753, 2019.
- [15] Julius Von Kügelgen, Yash Sharma, Luigi Gresele, Wieland Brendel, Bernhard Schölkopf, Michel Besserve, and Francesco Locatello. Self-supervised learning with data augmentations provably isolates content from style. *Advances in neural information processing systems*, 34:16451–16467, 2021.
- [16] Ting Chen, Simon Kornblith, Mohammad Norouzi, and Geoffrey Hinton. A simple framework for contrastive learning of visual representations. In *International conference on machine learning*, pages 1597–1607. PMLR, 2020.
- [17] Irina Higgins, Loic Matthey, Arka Pal, Christopher Burgess, Xavier Glorot, Matthew Botvinick, Shakir Mohamed, and Alexander Lerchner. beta-vae: Learning basic visual concepts with a constrained variational framework. In *International conference on learning representations*, 2016.

- [18] Xi Chen, Yan Duan, Rein Houthoofd, John Schulman, Ilya Sutskever, and Pieter Abbeel. Infogan: Interpretable representation learning by information maximizing generative adversarial nets. *Advances in neural information processing systems*, 29, 2016.
- [19] Ricky TQ Chen, Xuechen Li, Roger B Grosse, and David K Duvenaud. Isolating sources of disentanglement in variational autoencoders. *Advances in neural information processing systems*, 31, 2018.
- [20] Hyunjik Kim and Andriy Mnih. Disentangling by factorising. In *International Conference on Machine Learning*, pages 2649–2658. PMLR, 2018.
- [21] Abhishek Kumar, Prasanna Sattigeri, and Avinash Balakrishnan. Variational inference of disentangled latent concepts from unlabeled observations. In *International Conference on Learning Representations*, 2018.
- [22] Minyoung Kim, Yuting Wang, Pritish Sahu, and Vladimir Pavlovic. Bayes-factor-vae: Hierarchical bayesian deep auto-encoder models for factor disentanglement. In *Proceedings of the IEEE/CVF international conference on computer vision*, pages 2979–2987, 2019.
- [23] Michael F Mathieu, Junbo Jake Zhao, Junbo Zhao, Aditya Ramesh, Pablo Sprechmann, and Yann LeCun. Disentangling factors of variation in deep representation using adversarial training. *Advances in neural information processing systems*, 29, 2016.
- [24] Xuanchi Ren, Tao Yang, Yuwang Wang, and Wenjun Zeng. Rethinking content and style: exploring bias for unsupervised disentanglement. In *Proceedings of the IEEE/CVF International Conference on Computer Vision*, pages 1823–1832, 2021.
- [25] Xuanchi Ren, Tao Yang, Yuwang Wang, and Wenjun Zeng. Learning disentangled representation by exploiting pretrained generative models: A contrastive learning view. In *International Conference on Learning Representations*, 2021.
- [26] Shilong Liu, Lei Zhang, Xiao Yang, Hang Su, and Jun Zhu. Unsupervised part segmentation through disentangling appearance and shape. In *Proceedings of the IEEE/CVF Conference on Computer Vision and Pattern Recognition*, pages 8355–8364, 2021.
- [27] Gihyun Kwon and Jong Chul Ye. Diagonal attention and style-based gan for content-style disentanglement in image generation and translation. In *Proceedings of the IEEE/CVF International Conference on Computer Vision*, pages 13980–13989, 2021.
- [28] Zhizhong Wang, Lei Zhao, and Wei Xing. Stylediffusion: Controllable disentangled style transfer via diffusion models. In *Proceedings of the IEEE/CVF International Conference on Computer Vision*, pages 7677–7689, 2023.
- [29] Mohamad Harastani, Mikhail Eltsov, Amélie Leforestier, and Slavica Jonic. Hemnma-3d: cryo electron tomography method based on normal mode analysis to study continuous conformational variability of macromolecular complexes. *Frontiers in molecular biosciences*, 8:663121, 2021.
- [30] Mohamad Harastani, Mikhail Eltsov, Amélie Leforestier, and Slavica Jonic. Tomoflow: Analysis of continuous conformational variability of macromolecules in cryogenic subtomograms based on 3d dense optical flow. *Journal of molecular biology*, 434(2):167381, 2022.
- [31] Ellen D Zhong, Adam Lerer, Joseph H Davis, and Bonnie Berger. Cryodrgn2: Ab initio neural reconstruction of 3d protein structures from real cryo-em images. In *Proceedings of the IEEE/CVF International Conference on Computer Vision*, pages 4066–4075, 2021.
- [32] Axel Levy, Frédéric Poitevin, Julien Martel, Youssef Nashed, Ariana Peck, Nina Miolane, Daniel Ratner, Mike Dunne, and Gordon Wetzstein. Cryoai: Amortized inference of poses for ab initio reconstruction of 3d molecular volumes from real cryo-em images. In *European Conference on Computer Vision*, pages 540–557. Springer, 2022.
- [33] Kaiming He, Haoqi Fan, Yuxin Wu, Saining Xie, and Ross Girshick. Momentum contrast for unsupervised visual representation learning. In *Proceedings of the IEEE/CVF conference on computer vision and pattern recognition*, pages 9729–9738, 2020.
- [34] Yann LeCun. The mnist database of handwritten digits. <http://yann.lecun.com/exdb/mnist/>, 1998.
- [35] Stefan Hinterstoisser, Vincent Lepetit, Slobodan Ilic, Stefan Holzer, Gary Bradski, Kurt Konolige, and Nassir Navab. Model based training, detection and pose estimation of texture-less 3d objects in heavily cluttered scenes. In *Computer Vision—ACCV 2012: 11th Asian Conference*

- on *Computer Vision, Daejeon, Korea, November 5-9, 2012, Revised Selected Papers, Part I 11*, pages 548–562. Springer, 2013.
- [36] Alexandre Bône, Olivier Colliot, Stanley Durrleman, and Alzheimer’s Disease Neuroimaging Initiative. Learning the spatiotemporal variability in longitudinal shape data sets. *International Journal of Computer Vision*, 128(12):2873–2896, 2020.
- [37] Francesco Locatello, Stefan Bauer, Mario Lucic, Gunnar Raetsch, Sylvain Gelly, Bernhard Schölkopf, and Olivier Bachem. Challenging common assumptions in the unsupervised learning of disentangled representations. In *international conference on machine learning*, pages 4114–4124. PMLR, 2019.
- [38] Paul Wohlhart and Vincent Lepetit. Learning descriptors for object recognition and 3d pose estimation. In *Proceedings of the IEEE conference on computer vision and pattern recognition*, pages 3109–3118, 2015.
- [39] Steffen Klein, Mirko Cortese, Sophie L Winter, Moritz Wachsmuth-Melm, Christopher J Neufeldt, Berati Cerikan, Megan L Stanifer, Steeve Boulant, Ralf Bartenschlager, and Petr Chlanda. Sars-cov-2 structure and replication characterized by in situ cryo-electron tomography. *Nature communications*, 11(1):5885, 2020.
- [40] Irene de Teresa-Trueba, Sara K Goetz, Alexander Mattausch, Frosina Stojanovska, Christian E Zimmerli, Mauricio Toro-Nahuelpan, Dorothy WC Cheng, Fergus Tollervey, Constantin Pape, Martin Beck, et al. Convolutional networks for supervised mining of molecular patterns within cellular context. *Nature Methods*, 20(2):284–294, 2023.
- [41] Allison Doerr. Cryo-electron tomography. *Nature Methods*, 14(1):34–34, 2017.
- [42] PDB RCSB. Rcsb pdb, 2000.
- [43] Guang Tang, Liwei Peng, Philip R Baldwin, Deepinder S Mann, Wen Jiang, Ian Rees, and Steven J Ludtke. Eman2: an extensible image processing suite for electron microscopy. *Journal of structural biology*, 157(1):38–46, 2007.